TABLE 1 CP Performance for the Proposed Design in Figure 1; Antenna Parameters are Given in Figure 2; The Reference Antenna is for the Case of a Regular-Size CP Design (i.e., the Proposed Design without Inserted Slits)

	l (mm)	Δr (mm)	d_p (mm)	f_c (MHz)	Bandwidth (10 dB Return Loss)	CP Bandwidth (3 dB Axial Ratio)
Antenna 1	14.5	7.2	1.7	1805	3.13%	0.80%
Antenna 2	12	2.6	4.4	1977	3.21%	0.86%
Antenna 3	10	1.4	5.4	2115	3.27%	0.90%
Antenna 4	0	1.2	8.7	2560	6.50%	1.56%

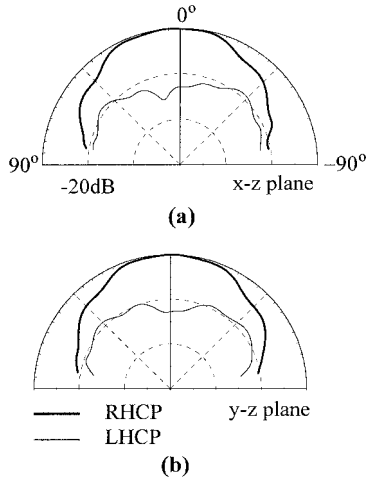

Figure 4 Measured radiation patterns in two orthogonal planes for antenna 1 given in Figure 2; $f = 1805$ MHz. (a) x–z plane. (b) y–z plane

Most important, from the results shown in Table 1, it is observed that the area of perturbation elements, the peripheral cuts at the patch boundary, for CP operation is significantly increased with increasing slit lengths or decreasing operating frequencies. This behavior is contrary to the results obtained for the compact CP design with a cross slot [3]. This suggests that fabrication tolerances for the present design are significantly relaxed, especially for the case with large slit lengths. Also, it is seen that the 50 Ω feed position moves close to the patch center when the slit length increases, similar to the case with a cross slot [3]. However, since the central portion of the patch in the present design is unslotted, there exists no restriction in locating the 50 Ω feed position when a large slit length is used. This characteristic makes it possible for the present design with a significantly lowered CP operating frequency; that is, a relatively larger antenna size reduction can be obtained for the present design. Figure 4 also shows the measured radiation patterns of antenna 1 in two orthogonal planes at the center operating frequency. From the results obtained, good right-hand CP radiation is observed.

4. CONCLUSIONS

A probe-fed circular microstrip antenna with four inserted slits at the patch boundary for achieving compact CP operation has been proposed and experimentally studied. Due to the central portion of the circular patch unslotted in the proposed antenna, the design in the present study allows easy location of the 50 Ω feed position for achieving compact CP operation. The fabrication tolerance is also much relaxed for the present design, especially for the condition of achieving large antenna size reduction at a fixed operating frequency. Results have also been obtained showing that, when compared to the regular-size CP design (unslotted patch case), the present proposed design can result in a reduction in the required antenna size as large as 50% for a given operating frequency.

REFERENCES

1. S.A. Bokhari, J.F. Zuercher, J.R. Mosig, and F.E. Gardiol, A small microstrip patch antenna with a convenient tuning option, IEEE Trans Antennas Propagat 44 (1996), 1521–1528.
2. K.L. Wong and J.Y. Wu, Single-feed small circularly polarised square microstrip antenna, Electron Lett 33 (1997), 1833–1834.
3. W.S. Chen, C.K. Wu, and K.L. Wong, Compact circularly-polarised circular microstrip antenna with cross-slot and peripheral cuts, Electron Lett 34 (1998), 1040–1041.

NUMERICAL MODELING AND EXPERIMENTAL INVESTIGATION OF RESONANCE PROPERTIES OF MICROWAVE CAPACITORS

Elena Semouchkina,[1] Wenwu Cao,[1, 2] Raj Mittra,[3] and Michael Lanagan[1]
[1] Materials Research Laboratory
The Pennsylvania State University
University Park, Pennsylvania 16802
[2] Department of Mathematics
The Pennsylvania State University
University Park, Pennsylvania 16802
[3] Department of Electrical Engineering
The Pennsylvania State University
University Park, Pennsylvania 16802

Received 23 October 2000

ABSTRACT: *The finite-difference time-domain (FDTD) field simulations have been employed to visualize standing-wave patterns in single-layer, rectangular, planar capacitors and capacitor chips. These patterns are used for the analysis of the resonant mode types, and for the determination of the resonance frequencies. The results of simulation are experimentally verified by measuring the S-parameter spectra. In addition, we show that the dimensions of the capacitor plates can be optimized in order to maximize the first resonant frequency of the capacitor, rendering it useful for high-frequency applications.* © 2001 John Wiley & Sons, Inc. Microwave Opt Technol Lett 29: 54–60, 2001.

Key words: *microwave capacitors; finite-difference time-domain method;*

Contract grant sponsor: Center for Dielectric Studies, Pennsylvania State University

1. INTRODUCTION

Investigation of the resonance properties of capacitors is very important for microwave applications [1]. As the operation frequency increases, the current flow in the interior of the capacitor is modified in a manner such that inductive effects are induced. In fact, at high frequencies, the capacitors behave like electromagnetic resonators, with undesirable resonances that degrade their performance. With the trend toward increasingly faster integrated circuits, it becomes necessary to search for better geometrical designs for capacitors in these circuits to push the resonant frequencies to higher values. Up to now, resonance processes in capacitors have not been analyzed using the advanced electromagnetic simulation techniques. Typically, capacitor designs are based on experience and approximating formulas that relate the geometry and material properties of a component to its characteristic parameters, such as capacitance, inductance, and resistance [2]. Such design approaches leave much to be desired in terms of accurately predicting the high-frequency characteristics of the capacitors. It is desirable, therefore, to analyze them using the more reliable electromagnetic simulation techniques.

The objective of this paper is to study resonance processes in single-layer planar capacitors and capacitor chips by using a powerful and general-purpose field solver, which is based on the finite-difference time-domain (FDTD) method. We compute the standing-wave patterns and determine associated resonance frequencies using the FDTD, and validate the results by comparing them with measured S_{11} spectra, which confirm that the resonance absorption occurs at the frequencies predicted by the standing-wave simulations. Our simulation approach is useful not only for understanding the resonance processes in capacitors, but also for finding optimum design geometries that provide improved performance at high frequencies.

2. SIMULATION PROCEDURE

We began by simulating the side-fed planar capacitor structures [see Fig. 1(a)] described in more detail in Section 3, which were also fabricated and measured experimentally. The excitation for the FDTD simulation was a Gaussian-shaped pulse, with a bandwidth of 15 GHz, which was modulated by a sinusoidal wave of 7.5 GHz. The structures were excited by applying the electric-field pulse between the microstrip feedline and the ground plane. Perfectly matched layers (PMLs) were employed at all truncation boundaries of the computational domains, except at the bottom surfaces, which were perfectly conducting ground planes.

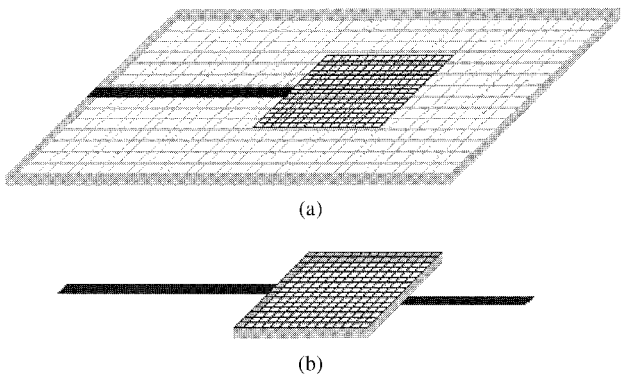

Figure 1 (a) Geometry of a planar capacitor. (b) Geometry of a capacitor chip

In addition, we have simulated single-layer capacitor chips [Fig. 1(b)], with the same dimensions and dielectric material properties as those of the planar capacitors. The simulated capacitor chips comprise two metal plates, with a dielectric layer inserted in between. They are surrounded by air, and have two feedlines attached to the two metal plates from different sides. No ground plane was placed at the bottom surface of the computational domain in this case, and the PML boundary condition was applied to all surfaces instead. The capacitor chips were excited by a Gaussian-shaped magnetic field pulse, which was applied around the input feedline [3].

The fast Fourier transformation (FFT) procedure was used to derive the electromagnetic fields in the frequency domain from the FDTD results, and the spatial electric-field distribution in the plane located below the metal plate inside the dielectric was computed. The frequency range was 0–18 GHz, and the step size was 0.1 GHz. Field plots were used to find the standing-wave patterns, and to determine the resonant frequencies of the structure. The latter were also determined from the simulation of the *S*-parameter spectra [4].

3. SAMPLES AND MEASUREMENTS

The planar capacitors were fabricated by using a standard thick-film process on alumina substrates. The relative dielectric constant of the substrate was equal to 9, and the dielectric layer thickness was 0.625 mm. The capacitor structure consists of a rectangular silver plate placed above the dielectric substrate and attached to a microstrip feedline [Fig. 1(a)], and its ground plane is located at the bottom of the substrate. This geometry was convenient for measuring the S_{11} spectrum. The metal pattern was created by screen printing conductive ink onto the substrate, and subsequently heat treating the assembly at 850°C.

Capacitors with three different plate dimensions, but with the same capacitor plate area of 72 mm^2, were fabricated. The plate dimensions (length $\times$ width) were (8×9) mm^2, (4.5×16) mm^2, and (6×12) mm^2, respectively. The length of the capacitor plate was measured in the direction of the input wave propagation, which was the direction of the feedline, while the width was measured in the perpendicular direction.

The scattering parameters S_{11} were measured as functions of frequency from 45 MHz to 18 GHz by using an HP8510C network analyzer. Spurious microwave reflections, occurring at the interface between the coaxial line and the microstrip, were accounted for by employing a standard two-port calibration procedure.

4. RESULTS

Figure 2 presents the distribution of the electric-field component normal to the substrate surface at the first resonance frequency for the (8×9) mm^2 planar capacitor fed symmetrically, with the feedline connected to the middle point of the left side of its plate [Fig. 1(a)]. The distribution is sampled in the plane located 0.25 mm below the metal plate inside the dielectric. The standing-wave pattern, which is characterized by the presence of field maxima and nulls, with wide swings in

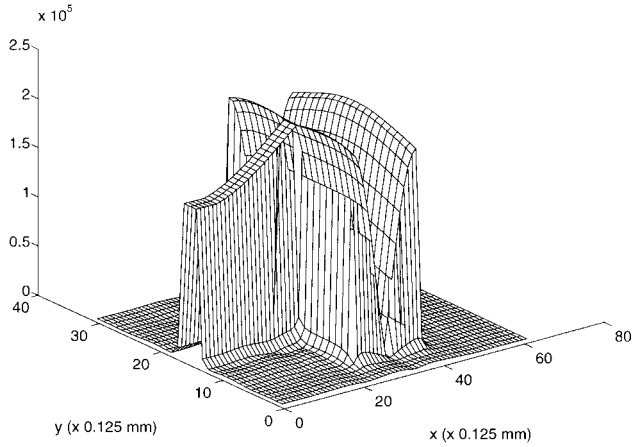

Figure 2 Distribution of the electric-field component normal to the substrate surface in the plane located 0.25 mm below the metal plate for the (8×9) mm^2 capacitor at the first resonance frequency of 5.8 GHz

the field magnitude and a symmetric field distribution, can be clearly seen in this plot.

Figures 3–5 are contour plots of the normal field component in the same plane as that in the previous case, at resonance frequencies, for three types of capacitor plate geometries, viz. (8×9) mm^2 (Fig. 1), (4.5×16) mm^2 (Fig. 2), and (6×12) mm^2 (Fig. 3). The observed standing-wave patterns correspond to resonant modes that can be "longitudinal," "transverse," or "mixed" types.

As seen in Figure 3, the lowest resonance frequency of the (8×9) mm^2 capacitor is associated with the "longitudinal" resonance, for which a half-wavelength standing wave is established in the direction of input wave propagation. We denote this resonance as {10} [Fig. 3(a)]. Our results of field simulation in the time domain have shown that the "transverse" resonances form independently in the two halves of the capacitor, which are symmetric to the strip-line axis; consequently, there is no {01}-type resonance in this case. Therefore, the second resonance corresponds to a two half-wavelength-type of standing wave, which is established in the direction perpendicular to the input wave propagation. We denote this type of resonance as {02} [see Fig. 3(b)]. Higher frequency resonances observed in the frequency range of investigation are {20}, {12}, {22}, and {30}, as shown in Figure 3(c)–(f). In this type of capacitor, the length of the capacitor plate exceeds one-half of its width.

Figure 4 presents the simulation results for a capacitor, whose plate dimensions are (4.5×16) mm^2, and hence, half of its plate width exceeds the plate length. The lowest resonance in this capacitor corresponds to the "transverse" {02} type [see Fig. 4(a)], where two half-wavelength standing waves are established in the direction perpendicular to the input wave propagation direction. The half-wavelength "longitudinal" standing wave of {10} type is observed at the second resonant frequency [Fig. 4(b)]. Other observed resonances correspond to {12}, {03}, {13}, and {04} modes, and are shown in Figure 4(c)–(f), respectively.

These results lead us to conclude that the optimum geometry of the symmetrically side-fed capacitor, which would provide the highest resonant frequency, is the one for which the plate length equals one-half of its width. Figure 5 presents the results of simulation for such a capacitor design, with plate dimensions of (6×12) mm^2. We observe from these plots that the first resonance in this capacitor indeed occurs at a frequency higher than those of the two previous geometries, and is of a "tandem" {t} type, which is different from the next "mixed" type resonance mode {12}. In fact, this {t}-type resonance mode is the superposition of the "longitudinal" and "transverse" resonance modes, which occur simultaneously at the same resonant frequency in both capacitor halves, located symmetrically to the strip-line axis [Fig. 5(a)]. The other resonances for this capacitor correspond to {12}, {20}, {03}, {22}, and {13} modes, respectively, and are shown in Figure 5(b)–(f).

The conclusion regarding the existence of optimal capacitor plate dimensions derived by our modeling approach is different from what has been generally accepted in the past (see, for example, [5]), which assumes that the inductance of the capacitor decreases and its resonance frequency increases monotonically with decreasing capacitor plate length and increasing width.

Figure 6(a)–(c) plots the measured (solid curves) and the computed (dashed curves) $|S_{11}|$-parameter spectra for the symmetrically side-fed capacitors, with plate dimensions similar to those in Figures 3–5. We find from these results that all of the resonances predicted by the simulated standing-wave patterns (Figs. 3–5) are indeed observed in the experimental spectra. In general, the simulated $|S_{11}|$ spectra agree well with the measured data. However, the pure "longitudinal" and "transverse" resonances are more pronounced in the simulated spectra than the "mixed"-type resonances, while the "mixed" resonances produce deeper minima in the measured spectra.

It is worthwhile mentioning at this point that the proposed standing-wave pattern approach for determining the resonant frequencies of the structure presents a distinct advantage over the S-parameter simulation technique because we only need 3000 time steps in the FDTD simulation (a time step is equal to 0.24 ps) to realize well-established standing-wave patterns, while the S-parameter spectra simulations require at least 25,000 time steps for the signals to fully decay within the circuit [4], which is necessary for accurate estimation of the resonant frequencies.

The simulations of the capacitor chips showed that the standing-wave patterns for three different plate geometries of symmetrically fed capacitor chips are similar to the ones for planar capacitors when the plate dimensions are identical. For instance, the highest resonance frequency in capacitor chips was observed when the length-to-width ratio was 1:2 both for capacitor chips and planar capacitors, although the resonant frequencies of the former were slightly higher.

It is interesting to note that Napoli and Hughes [6], who have investigated rectangular waveguides with open-circuited sidewalls, have suggested the existence of modes similar to the ones we found in planar and chip capacitors. The possible existence of modes of this type has also been mentioned in the context of patch antenna designs [7].

5. CONCLUSION

The FDTD simulations enabled us to visualize and analyze the standing-wave formation in single-layer rectangular plate capacitors, and to define the optimum geometry design for high-frequency applications. The optimum length of the plate for the symmetrically side-fed capacitor was found to equal one-half of its width. The simulation results were verified by

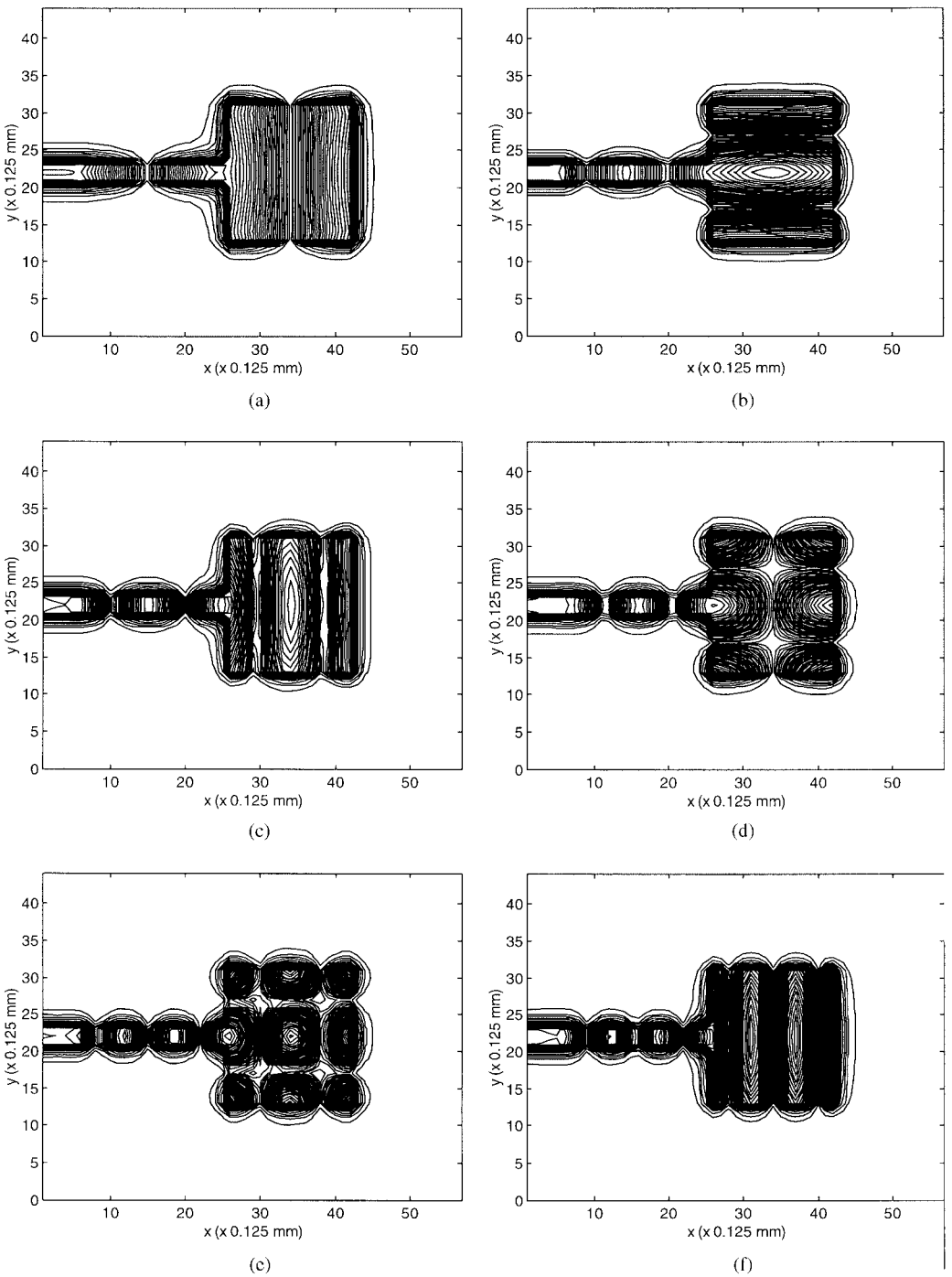

Figure 3 Contour plots of the electric-field component normal to the substrate surface in the plane located 0.25 mm below the metal plate for the (8×9) mm^2 capacitor at different resonance frequencies: (a) -5.9 GHz {10}, (b) -10.2 GHz {02}, (c) -11.5 GHz {20}, (d) -12.3 GHz {12}, (e) -15.9 GHz {22}, (f) -16.8 GHz {30}

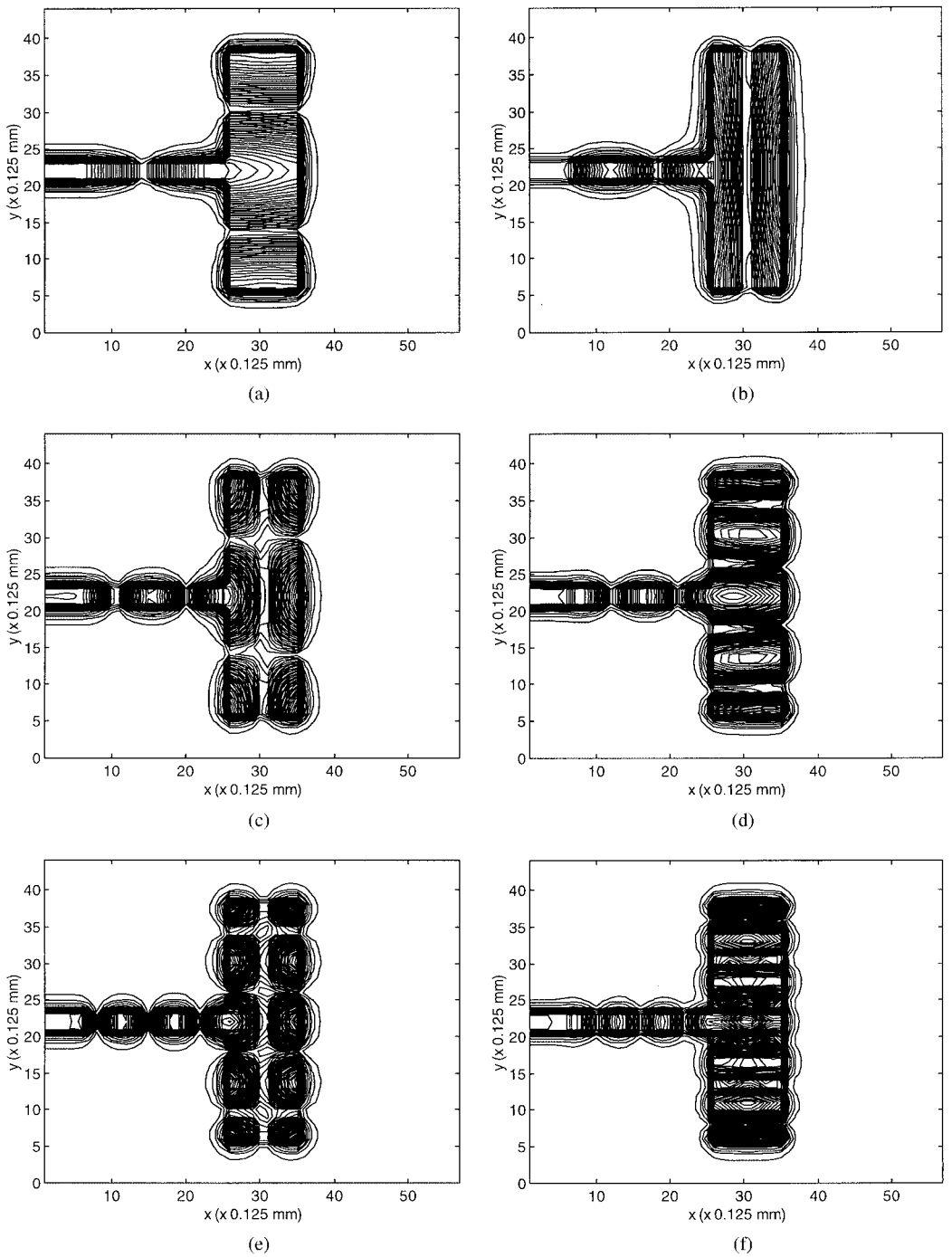

Figure 4 Contour plots of the electric-field component normal to the substrate surface in the plane located 0.25 mm below the metal plate for the (4.5×16) mm^2 capacitor at different resonance frequencies: (a) -6.2 GHz {02}, (b) -9.2 GHz {10}, (c) -11.5 GHz {12}, (d) -12.3 GHz {03}, (e) -16 GHz {13}, (f) -18 GHz {04}

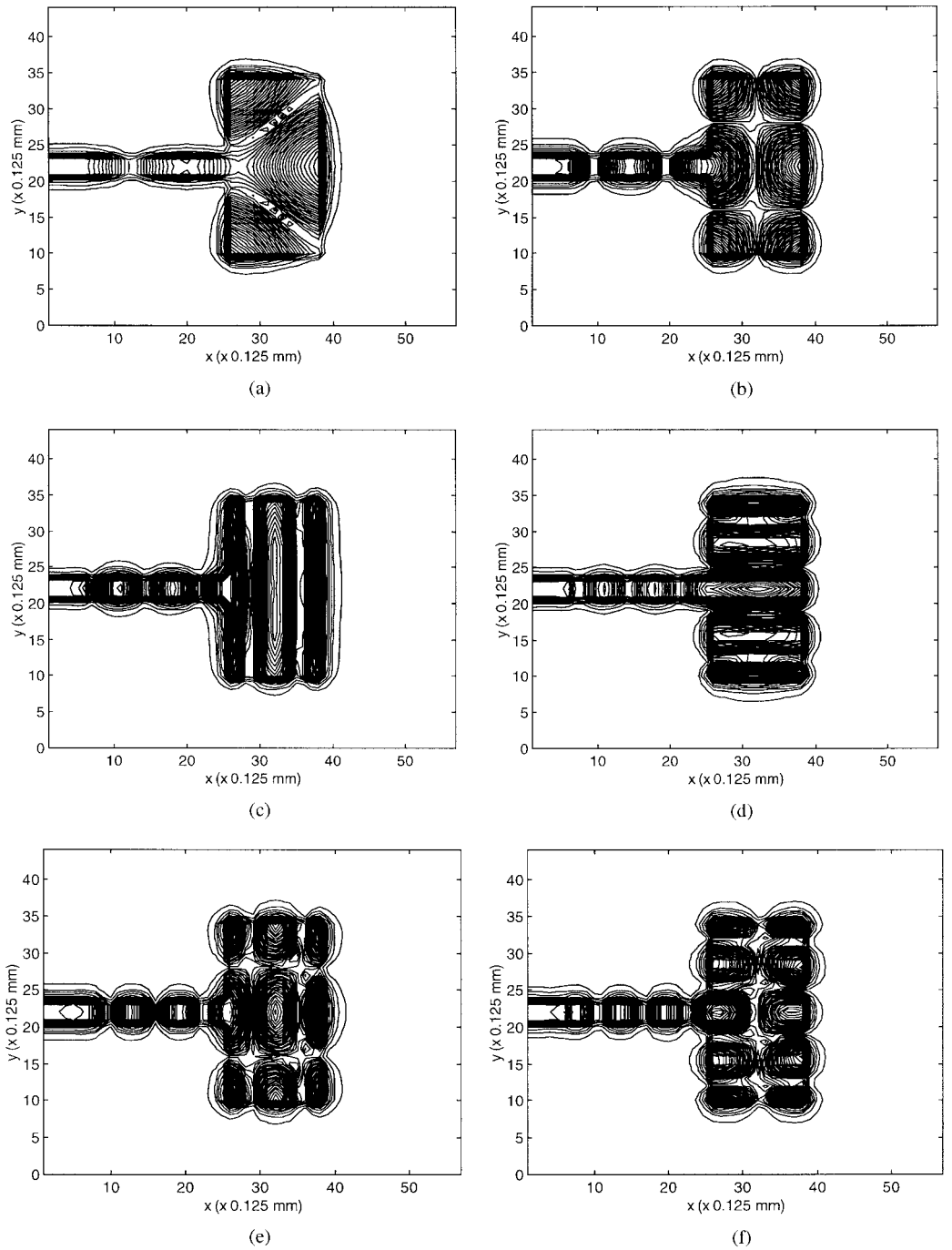

Figure 5 Contour plots of the electric-field component normal to the substrate surface in the plane located 0.25 mm below the metal plate for the (6×12) mm^2 capacitor at different resonance frequencies: (a) -7.8 GHz {*t*}, (b) -11.4 GHz {12}, (c) -14.6 GHz {20}, (d) -15.8 GHz {03}, (e) -17.0 GHz {22}, (f) -17.9 GHz {13}

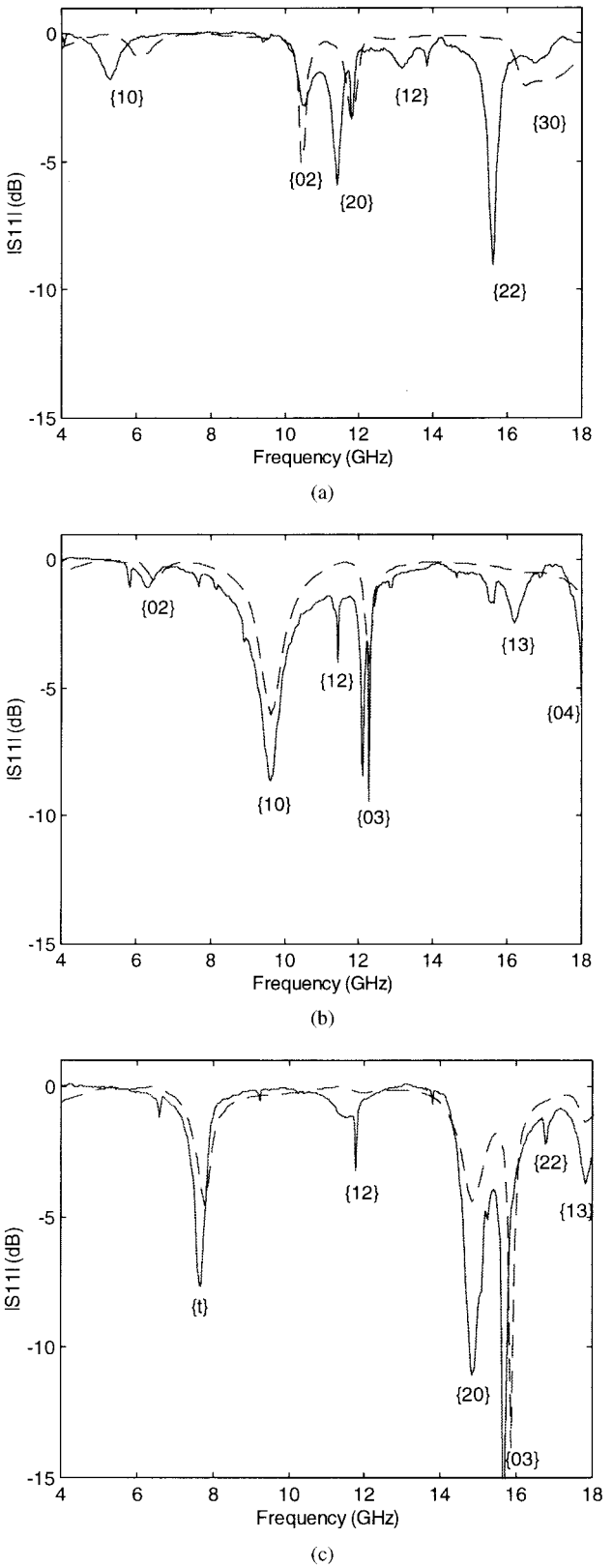

Figure 6 Simulated (dashed curves) and measured (solid curves) $|S_{11}|$-parameter spectra for the capacitors with plate dimensions of (a) (8×9) mm^2, (b) (4.5×16) mm^2, and (c) (6×12) mm^2, respectively

the measurements of S_{11}-parameter spectra of planar capacitors, and good agreement was found.

ACKNOWLEDGMENT

The authors would like to thank Amanda Baker for sample fabrication, and Steve Perini for device measurements.

REFERENCES

1. A.T. Murphy and F.J. Young, High frequency performance of multilayer capacitors, IEEE Trans Microwave Theory Tech 43 (1995), 2007–2015.
2. N. Coda and J.A. Salvaggi, Design consideration for high-frequency ceramic chip capacitors, IEEE Trans Parts, Hybrids, Pack, PHP-12 (1976), 206–212.
3. E. Semouchkina, W. Cao, and R. Mittra, Source excitation methods for the finite-difference time-domain modeling of circuits and devices, Microwave Opt Technol Lett 21 (1999), 93–100.
4. E. Semouchkina, W. Cao, and R. Mittra, Modeling of microwave ring resonators using the finite-difference time-domain (FDTD) method, Microwave Opt Technol Lett 24 (2000), 392–396.
5. O. Boser and V. Newsome, High frequency behavior of ceramic multilayer capacitors, IEEE Trans Comp, Hybrids, Manufact Technol CHMT-10 (1987), 437–439.
6. L.S. Napoli and J.J. Hughes, A simple technique for the accurate determination of the microwave dielectric constant for microwave integrated circuit substrates, IEEE Trans Microwave Theory Tech MTT-19 (1971), 664–665.
7. J.A. Navarro and K. Chang, Integrated active antennas and spatial power combining, Wiley, New York, 1996, chap. 7, p. 142.

COMPACT DUAL-FREQUENCY DUAL-POLARIZED SLOTTED MICROSTRIP PATCH ANTENNA

G. S. Binoy,[1] C. K. Aanandan,[1] P. Mohanan,[1] and K. Vasudevan[1]
[1] Center for Research in Electromagnetics and Antennas
Department of Electronics
Cochin University of Science & Technology
Cochin-22, Kerala, India

Received 16 October 2000

ABSTRACT: *A new design for the compact single-feed dual-frequency operation of a slotted square microstrip antenna is demonstrated. The antenna generates two distinct operating frequencies with different polarization planes and broad radiation characteristics. The antenna has the added advantage of an antenna size reduction as large as ~61 and 45% in comparison to the standard rectangular patch for the above two frequencies.* © 2001 John Wiley & Sons, Inc. Microwave Opt Technol Lett 29: 60–62, 2001.

Key words: *dual frequency; slotted; square microstrip; dual polarized*

INTRODUCTION

Dual-frequency microstrips generally have applications in which different frequencies are used for transmission and reception, such as personal satellite communications and cellular network systems. Also, wide attention has been attained by microstrip slot antennas owing to their better impedance matching and dual-frequency operation. A variety of dual-band microstrip patch antennas are available in the literature. A dual-frequency dual-polarized simple rectangu-